

Novel algorithms for efficiently
accumulating, analysing and
visualising full-waveform LiDAR in
a volumetric representation with
applications to forestry

submitted by

Milto Miltiadou

for the degree of Doctor of Engineering

of the

University of Bath

Centre for Digital Entertainment

and of the

Plymouth Marine Laboratory

NERC Airborne Research Facility

April 2017

COPYRIGHT

Attention is drawn to the fact that copyright of this thesis rests with its author. This copy of the thesis has been supplied on the condition that anyone who consults it is understood to recognise that its copyright rests with its author and that no quotation from the thesis and no information derived from it may be published without the prior written consent of the author.

This thesis may be made available for consultation within the University Library and may be photocopied or lent to other libraries for the purposes of consultation.

Signature of Author.....

Milto Miltiadou

Abstract

no more than 300 words

NOTES:

Blue colour: additions according to Neill's feedback,

Purple colour: addition/corrections according to Mike's comments

Red colour: notes

Gray colour: text that is going to be modified

To be added on top

Abstract

This study focuses on enhancing the visualisations and classifications of forested areas using coincident full-waveform (fw) LiDAR data and hyperspectral images. The ultimate aim is use both datasets to derive information about forests and show the results on a 3D virtual, interactive environment. Influenced by Persson et al (2005), voxelisation is an integral part of this research. The intensity profile of each full-waveform pulse is accumulated into a voxel array, building up a 3D density volume. The correlation between multiple pulses into a voxel representation produces a more accurate representation, which confers greater noise resistance and it further opens up possibilities of vertical interpretation of the data. The 3D density volume is then aligned with the hyperspectral images using a 2D grid similar to Warren et al (2014) and both datasets are used in visualisations and classifications.

Previous work in visualising fw LiDAR has used transparent objects and point clouds, while the output of this system is a coloured 3D-polygon representation, showing well-separated structures such as individual trees and greenhouses. The 3D density volume, generated from the fw LiDAR data, is polygonised using functional representation of object (FReps) and the marching cubes algorithm (Pasko and Savchenko, 1994) (Lorensen and Cline, 1987). Further, an optimisation algorithm is introduced that uses integral volumes (Crow, 1984) to speed up the process of polygonising the volume. This optimisation approach not only works on non-manifold object, but also a speed up of up to 51% was achieved. The polygon representation is also textured by projecting the hyperspectral images into the mesh. In addition, the output is suitable for direct rendering with commodity 3D-accelerated hardware, allowing smooth visualisation.

In future work, the effects of combining both hyperspectral imagery and fw LiDAR in classifications and visualisations are examined. At first, two pixel wise classifiers, a support vector machine and a Bayesian probabilistic model, will be used for testing the effects of the combination in generating tree coverage maps. Higher accuracy classification results are expected when metrics from both datasets are used together. Regarding the visualisations, the differences of applying surface reconstruction versus direct volumetric rendering will be discussed and an ordered tree structure with integral sums of the node values will be used for speeding up the ray-tracing of direct volumetric rendering and improving memory management of aforementioned optimisation algorithm with integral volumes. Further, deferred rendering is suggested for testing the visual human perception of projecting multiple bands of the hyperspectral images on the FW LiDAR

polygon representations. At the end of this project the combination of the datasets will be used along with the watershed algorithm for tree segmentation, which is useful for measuring the stem density of a forest and for tree species classifications.

from EDE:

Firstly, a new and fast way of aligning the FW LiDAR with Remotely Sensed Images has been developed in DASOS and by generating tree coverage maps it was shown that the combination of those datasets confers better remote survey results. This work was presented at the 36th ISRSE International Conference.

Secondly, automated detection of dead trees in native Australian forests has a significant role in protecting animals, which live in those trees and are close to extinction. DASOS allow the generation of 3D signatures characterising dead trees. A comparison between the discrete and FW LiDAR is performed to demonstrate the increased survey accuracy obtained when the FW LiDAR are used.

Finally, the last application is for improving visualisations for foresters. Foresters have a great knowledge about forests and can derive a wealth of information directly from visualisations of the remotely sensed data. This reduces the travelling time and cost of getting into the forests. This research optimises visualisations by using the new FW LiDAR representations and a speed of up to 51% has been achieved.

FW LiDAR has great potentials in forestry and this research has already started to have an impact in the FW LiDAR community by making those huge datasets easier to handle. DASOS is now used at Interpine Group Ltd, a world leading Forestry Company in New Zealand and it has been tested from a PhD student at Bournemouth University who looks into estimating bird distribution in the New Forest. In the future, it is expected that DASOS will be widely used in remote forest surveys (i.e. estimating the commercial value of a forest and detecting infected trees at early stages for treatment).

Acknowledgements

Above all, I would like to express my great gratitude to my industrial supervisors Dr. Michael Grant who had supported me continuously during my research and gave me the freedom to create a project of my own interest.

Then, I would like to thanks Dr. Matthew Brown, who helped me during my first years of my studies by giving me valuable and informative feedback. He was always there to keep me working on the right track.

Equally important is my current supervisor Dr. Neil D.F. Campbell and he is not to be missed from the acknowledgements.

Furthermore, special thanks are given to Dr. Mark Warren, Dr. Darren Cosker, MSc Susana Gonzalez Aracil and Dr. Ross Hill who occasionally advised me during my studies.

It further worth giving credits to my data providers, the Natural Environment Research Council's Airborne Research Facility (NERC ARF) and Interpine Group Ltd.

Last but not least, I am extremely grateful to my funding organisations, the Centre for Digital Entertainment and Plymouth Marine Laboratory, who supported financially and consequently made this research possible.

Abbreviations and Glossary

AGC	Automatic Gain Controller
ALS	Airborne Laser Scanning
APL	Airborne Processing Library
ARF	Airborne Research Facility
CG	Computer Graphics
CHM	Canopy Height Model
CUDA	parallel computing platform available on nvidia graphic cards
DASOS	(δασος=forest in Greek), the open source software implemented for managing FW LiDAR data
DBH	Diameter at Breast Height
DEM	Digital Elevation Model
DTM	Digital Terrain Model (DTM)
FW	Full-Waveform
GB	Gigabyte
GPU	Graphics Processing Unit
LiDAR	Light Detection And Ranging
MRI	Magnetic Resonance Imaging
NASA	National Aeronautics and Space Administration
NDVI	Normalised Difference Vegetation Index
NERC	Natural Environment Research Council
NIR	Near-Infrared Region of the electromagnetic spectrum
QGIS	Quantum Geographic Information System
SIMD	Single Instruction, Multiple Data
TB	Terabyte
VIS	Visual Spectrum
VLR	Variable Length Records
WPDF	Waveform Packet Descriptor Format
UK	United Kingdom

Publications

DASOS-User Guide, M. Miltiadou, N.D.F Campbell, M. Brown, S.C. Aracil, M.A. Warren, D. Clewley, D.Cosker, and M. Grant, Full-waveform LiDAR workshop at Interpine Group Ltd, Rotorua NZ, 2016

Improving and Optimising Visualisations of full-waveform LiDAR data, M. Miltiadou, M. Brown, N.D.F Campbell, D. Cosker, M. Grant, *EuroGraphics UK, Computer Graphics & Visual Computing*, 2016

University of Bath Alignment of Hyperspectral Imagery and Full-Waveform LiDAR data for visualisation and classification purposes, M. Miltiadou, M. A. Warren, M. Grant, and M. Brown, *The International Archives of Photogrammetry, Remote Sensing and Spatial Information Sciences*, vol. 40, no. 7, p. 1257, 2015.

Reconstruction of a 3D Polygon Representation from Full-Wavefrom LiDAR data, M. Miltiadou, M. Grant, M. Brown, M. Warren, and E. Carolan,*RSPSoc Annual Conference, New Sensors for a Changing World*, 2014.

Awards

EDE and Ravenscroft Prize - Finalist: Selected as one of the five finalists for this is a prestigious prize that recognises the work of best postgraduate researchers.

Student Poster Competition at Silvilaser.

Conference Presentations

Remote Sensing Cyprus (RSCy) Conference, 2017 , Paphos, Cyprus - Oral Presentation

ForestSAT Conference,2016 , Santiago, Chile - Oral Presentation

Computer Graphics & Visual Computing (CGVC),2016, Bournemouth, United Kingdom - Poster Presentation

Silvilaser, 2015, La Grant Motte, France - Oral Presentation

International Symposium of Remote Sensing of the Environment (ISRSE), 2015, Berlin, German - Oral Presentation

Remote Sensing and Photogrammetry Society (RSPSoc) Conference, New Sensors for a Changing world , 2014, Aberystwyth, United Kingdom - Oral Presentation

Workshops

Full day workshop about FW LiDAR and DASOS at *Interpine Ltd Group*, 2016,
Rotorua, New Zealand

Demonstration of DASOS_v2 at the practical LiDAR session at *the NERC ARF annual workshop*, 2017, Plymouth, United Kingdom

Contents

Abstract	i
Acknowledgements	iii
Abbreviations and Glossary	iv
Publications	v
Awards	v
Conference Presentations	v
Workshops	vi
List of Figures	ix
1 Introduction	1
1.1 Forest Monitoring: Importance and Applications	1
1.2 Background Information about Remote Sensing and Airborne Laser Scanning Systems	1
2 Acquire Data	3
2.1 Airborne LiDAR systems: An in-depth Explanation	5
2.2 Brief Description of the LAS1.3 File Format	6
2.3 Leica Vs Trimble Instruments: Limitations, Differences and Advantages	6
2.4 Hyperspectral Imagery	8
3 Overview of Thesis	11
4 The open source software DASOS and the Voxelisation Approach	12
4.1 State-of-Art FW LiDAR Software Packages	12
4.2 Voxelisation for Interpreting FW LiDAR data	15
4.3 The functionalities of DASOS	17
4.4 Summary and Discussion	22
5 Surface Reconstruction from Voxelised FW LiDAR Data	23

6 Optimisation Attempts for the Surface Reconstruction	24
7 Alignment with Hyperspectral Imagery	25
8 Detection of Dead Standing Eucalyptus For Managing Biodiversity in Native Australian Forest	26
9 Overall Results	27
10 Conclusions	28
10.1 Contributions	29
Bibliography	29
A DASOS user guide	i
B Case Study: Field Work in New Forest	ii

List of Figures

2-1	Data and Instruments	4
2-2	Airborne Laser Scanning System	4
2-3	LAS1.3 File Format	7
2-4	Hyperpsectral Cube	10
4-1	Voxelisation of FW LiDAR data	16
4-2	Example of .csv files with priors exported. These priors contain the raw intensities of the voxels.	21
4-3	Example of .csv files with priors exported. These priors contains processed information about the the local area of interest (i.e. spread of non empty voxels).	21

Chapter 1

Introduction

1.1 Forest Monitoring: Importance and Applications

1.2 Background Information about Remote Sensing and Airborne Laser Scanning Systems

Remote sensing refers to the acquisition of information about objects, for example vegetation and archaeological monuments, without physical contact and the subsequent interpretation of that information. The sensors used to capture the information are divided into passive and active. For example satellite photography is passive because information are collected from the reflected natural sun light, while Airborne Laser Scanners (ALS) are active because they emit laser beams and collects information from the backscattered laser energy [1].

According to Wanger et al, Airborne Laser Scanning (ALS) is a growing technology used in environmental research to collect information about the Earth, such as vegetation and tree species. Comparing ALS with traditional photography, ALS is not influenced by light and it is therefore less dependent on weather conditions (ie. it collects information from below the clouds, or at night). The laser beam also partially penetrates the tree canopies allowing it to record information about the forest structure below the canopy, as well as the ground [2]. ALS methods are divided into pulse systems, which repeatedly emit pulses, and continuous wavelength systems that continuously emit light. They both acquire information from the backscattered laser intensity over time, but continuous wavelength systems are more complicated because they obtain one extra physical parameter, the frequency of the ranging signal. Further, according to Wehr and Lohr, continuous wavelength systems are 85 times less accurate than pulse systems [3].

LiDAR (Light Detection And Ranging) systems are active and pulse laser scanning systems [3]. They are divided into two groups according to the diameter of the footprint left by the laser beam on the ground, which is primarily dependent on the distance between the sensor and the target (altitude, in most remote sensing) and the beam divergence. The small-footprint group has a 0.2-3m diameter, is widely commercialised and the sensors are mostly carried on planes (ALS systems). In contrast, the large-footprint systems have a wider diameter (10-70m) and during experiments they were mostly mounted on satellites. Small-footprint systems record at higher resolution but cannot guarantee that every pulse will reach the ground due to the small diameter of their footprint, making topographic measurements difficult, and are limited to smaller survey areas due to the cost and availability of aircraft. In contrast, large-footprint scanners have wider diameters and can therefore scan wider areas with the likelihood of recording the ground to be higher [4].

In addition, there are two types of LiDAR data: discrete and full-waveform (FW). Discrete LiDAR records a few peaks of the reflected laser intensity, while FW LiDAR stores the entire backscattered signal. The discrete LiDAR has been widely used and a 40% reduction of fieldwork has been achieved at Interpine Ltd Group, New Zealand, with that technology. Regarding the newer FW LiDAR, scientists understand their concepts and potentials but due to the shortage of available tools able to handle these large datasets, there are very few uses of FW LiDAR [5].

The design of the first FW LiDAR system was introduced in 1980s, but the first operational system was developed by NASA in 1999 [6]. The vastly increased amount of information recorded within the FW LiDAR suggests many new possibilities and problems from the point of view of image understanding, remote surveying and visualisation. As an indication, a 9.3GB discrete LiDAR from New Forest, UK, corresponds to 55.7GB of FW LiDAR.

This research is focused on the representation and efficient use of FW LiDAR data and contributes both to forestry visualisations and classifications. Two datasets are used for testing and evaluation: the New Forest and the RedGum dataset. An in-depth explanation of LiDAR systems and the specifications, differences and challenges of the two datasets are given in Section 2. An overview of the specific aims, objectives and contributions of this thesis, set in the context of these datasets, is then given at Section 3.

Chapter 2

Acquire Data

The aim of this section is to give a practical and scientific insight into the acquisition of data, because a good knowledge of these methods and their limitations is essential for understanding the related research undertaken. The relations between the two main datasets used in this project are depicted on Figure 2-1 and briefly explained here:

- The **New Forest dataset** from the UK was provided by the Natural Environment Research Council's Airborne Research Facility (NERC ARF). Measurements were collected simultaneously a Leica ALS50-II LiDAR and AISA Eagle/Hawk hyperspectral radiometers on the 8th of April in 2010. It contains Discrete LiDAR, FW LiDAR and hyperspectral images.
- The **RedGum dataset** was acquired in Australia using a Trimble AX60 integrated LiDAR/Camera instrument over the time period from the 6th of March in 2015 until the 31st of March in 2015. It was provided by the RPS Australia East Pty Ltd. Only the FW LiDAR data are used here.

The ALS data are explained first, because they are the main focus of this research, and hyperspectral imagery is towards the end of the chapter. In Section 2.1, an in-depth description of ALS systems and the differences between discrete and FW LiDAR data is given. Section 2.2 briefly discusses the binary file format of the acquired LiDAR data and Section 2.3 is a discussion on the limitations, the differences and the advantages of two LiDAR instruments; the Leica and Trimble. The essential information about the hyperspectral imagery, which is only associated with the New Forest dataset, is then covered in Section 2.4.

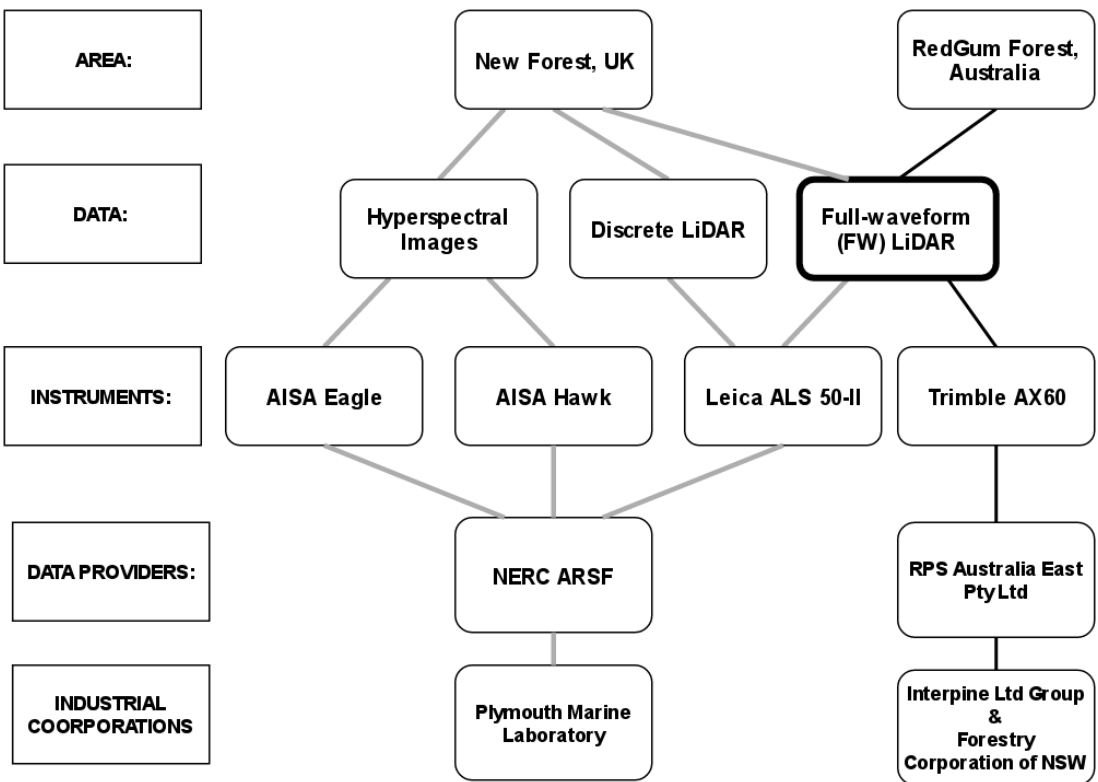


Figure 2-1: Data and Instruments

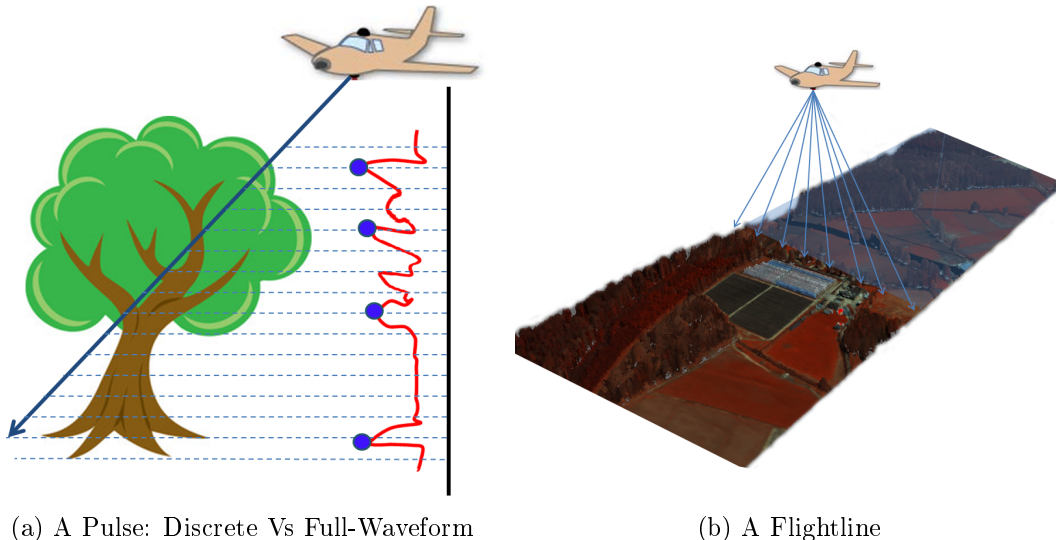


Figure 2-2: Airborne Laser Scanning System

2.1 Airborne LiDAR systems: An in-depth Explanation

The ALS systems emit laser pulses from sensor mounted in a plane and collects information from the time-of-flight and the returned laser intensity. By the time the pulse has travelled the approximately 1-3km from the aircraft to the ground, it is roughly 20cm in width due to beam divergence. When the pulse hits an object (e.g. the forest canopy), then some of it reflects back while the rest penetrates through holes between leaves and branches. The laser pulse continues to hit structures, scattering and partially returning to the sensor until it reaches a solid barrier such as the ground and is fully blocked from further progress. The LiDAR systems record information from the backscattered laser pulse, measuring its round trip time and the returned intensity.

As mentioned at Section 1.2, there are two types of LiDAR data, discrete and FW. The discrete LiDAR observes the returned intensity signals and identifies and [records a few peak intensity returns of the signal](#), while the FW LiDAR system digitises and stores the entire backscattered signal into equally spaced time intervals (Figure 2-2a). The delivered data for the discrete LiDAR is a set of hit points ("returns"), which are associated with laser intensities. The world position of every return is calculated by measuring the round trip time of the laser return, giving a distance from the sensor, which is combined with the precisely known position and orientation of the aircraft/sensor (from GPS, an inertial measurement unit and precise shot direction of the laser pulse). The waveform recordings are triggered by and attached to first returns of discrete LiDAR data (to avoid sampling the uninteresting time period while the pulse travels through the atmosphere) and they are a list of intensities that correspond to the laser intensity returned over time. There is also an offset vector which defines the distance and direction between each wave sample (effectively a compression mechanism, by avoid recording the world position of every sample, replacing it with the location of the first return and this vector).

As shown in Figure 2-2b, the pulses are scanned back and forth across the landscape below (by a rotating mirror) as the plane travels forward. The scanned data has a limited maximum width according to the flight height and the field of view scan angle. During processing the track of the plane is divided into easier-to-handle pieces (flightlines) and saved into separate binary files. In this project the LAS1.3 file format is used for both datasets.

2.2 Brief Description of the LAS1.3 File Format

There are a few LiDAR file formats but the LAS1.3 was the first format to contain FW data and it is the one used to store the data for both New Forest and RedGum datasets. According to the LAS1.3 file specifications [7], a .LAS file contains information about both discrete and FW LiDAR data, with the waveform packets attached to discrete returns and saved either internally at the end of the .LAS file or externally in a .WVS file.

As shown at (Figure 2-3) the .LAS file is divided into four sections and a brief explanation of each section is given here:

1. The **Header** contains general information about the entire flightline. For example, it includes the maximum scan angle used during the flight, whether the waveform packets are recorded internally or externally and the number of **Variable Length Records** (VLR).
2. Regarding the **VLR**, which contain arbitrary "extension" data blocks, the most important information given is the waveform packet descriptors that contain essential information on how to read the waveform packets (i.e. an ID, the number of wave samples and the size of each intensity in bits).
3. The **Point Data Records** are the discrete points and the waveforms are associated with first return discrete points. Each Point Data Record has a spatial location, an intensity and optionally a pointer to a waveform packet as well as the ID of the corresponding waveform packet descriptor.
4. The waveform packets is a list of intensities and they are either saved internally into the **Extended Variable Length Records** section of the .LAS file or inside an external .WVS file. Starting from the associated first return point, the spatial locations of the waveform packet (wave sample intensity) are calculated by adding an offset defined in the associated Point Data Record.

2.3 Leica Vs Trimble Instruments: Limitations, Differences and Advantages

As shown in Figure 2-1, the Leica ALS 50-II instrument was used to capture the LiDAR data of New Forest dataset and the Trimble AX60 for collecting the RedGum Forest FW LiDAR data. It is therefore important to clarify the differences, the limitations and the advantages of each instrument.

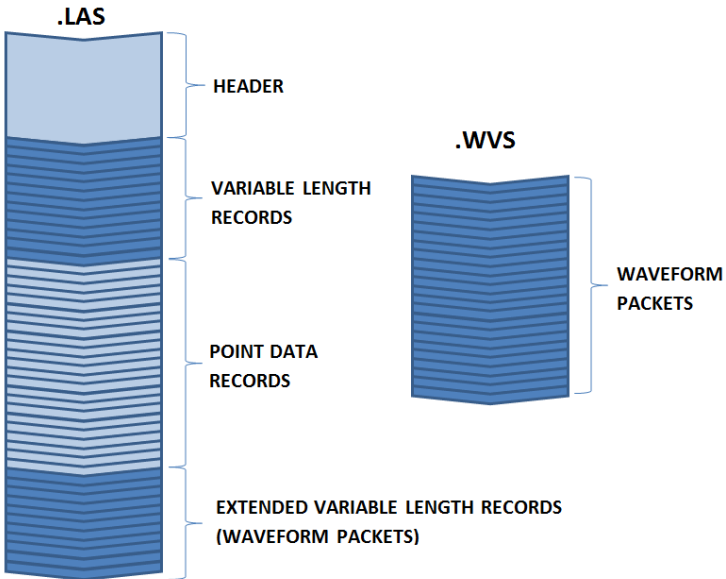


Figure 2-3: How the FW LiDAR data are stored into a binary file, according to the LAS1.3 file format specification

The Trimble performs at a pulse frequency of 400kHz, while the Leica's maximum pulse frequency is 120kHz. Nevertheless, during experiments there were occasions when the Leica discarded every other waveform due to I/O limitations despite being at or below the maximum pulse frequency [8]. The New Forest dataset has been affected by this and, on average, one third of the saved pulses only contain discrete data. We should therefore be extremely careful when comparing Discrete with FW LiDAR data. While [5] concludes that FW LiDAR data worth the extra processing because they have a better vertical profile, [9] states that extra information (the echo-width) from the FW LiDAR data are relatively unimportant. But the New Forest datasets were used for the comparison at [9] and there is no mention about the significantly less waveforms recorded in comparison to the discrete data. It is therefore suspected that their results has been affected by the missing waveforms.

Another problem with the Leica sysyem is the small dynamic range of intensities due to the number of bits used for recording them; the Leica system uses 8-bit integers (0-255 range) while the Trimble uses 16-bit integers (0-16385 range). For increased dynamic range and finer intensities without doubling storage costs, Leica introduced an Automatic Gain Controller (AGC). The AGC is an 8-bit number that defines how the recorded intensity range is shifted across a wider range of intensities. The AGC value is adjusted according to the reflected laser intensity of the previous 64 pulses and it therefore varies across a flightline. Consequently, the raw intensities are incomparable

to each other and, since the relation between AGC and the intensities is not linear, the range normalisation is complicated [10] [11]. In this thesis, the intensities of the Leica system are used as boolean values (whether something existed or not, using a user-defined threshold) to quickly overcome that issue and focus on the major research objectives. Regarding the Trimble instrument, there is no AGC value because the intensities are saved into a 16bit integer and as long as the flight height is constant no normalisation is required. In a few words, the raw intensities recorded using the Leica system are not normalised and therefore not comparable to each other, while the intensities of the Trimble instrument are more meaningful.

The footprint of the laser on the ground depends on the scanning pattern of the instruments and the field of view. The sinusoidal scanning pattern of the Leica system results in a higher density of returns at the edges of the flightline. The footprint of the Trimble instrument is more equally spaced because they are scanned using a rotating polygon. The uneven density pattern of the Leica system is resolved by normalisation during the voxelisation process, but the Trimble's equally spaced pulse pattern is more prone to aliasing when voxelised. Regarding the field of view, the Leica is wider but both systems avoid large angles because otherwise data look deformed at edges of the flightlines.

Last but not least, the Trimble instrument is a native full-waveform sensor; the discrete LiDAR are produced by extracting peak points in post-processing. Therefore one of the purported advantages of a FW system, the concept of extracting a denser point clouds using Gaussian decomposition [2], does not apply in the Trimble's case. This was proven by extracting peak points from Trimble FW LiDAR data using the pulseextract from LAStools [12]; the number of points extracted was exactly the same as the number of points saved into the associated discrete LiDAR files. Therefore discrete data from the Trimble instrument are the same as those generated by echo decomposition and peak points extraction from the FW samples.

To sum up, the Trimble AX60 instrument is a newer sensor and therefore has less problems or design compromises in comparison to the Leica ALS50-II instrument. Table 2.1 summarises the differences between the two sensors.

2.4 Hyperspectral Imagery

Hyperspectral imagery has a positive impact in remote sensing because it contains information beyond human visibility. The human eye receives light from the visual spectrum into three bands (red, green and blue). The hyperspectral sensors captures a larger spectrum and divides its light components into hundreds of bands, recording

Table 2.1: Specifications of the LiDAR instruments used

Instrument Name:	Leica ALS550-II	Trimble Ax60
Scanned Area	New Forest, UK	RedGum, Australia
Year of Introduction:	Discrete LiDAR 2009 & FW LiDAR 2010	2013
Max Scan Frequency (kHz):	120	400
Recorded Intensity (bits):	8	16
AGC:	Yes	No
Scanning Pattern:	Sinusoidal	The footprints are more equally spaced on the ground
Max field of view (degrees):	75	60

this way more information than a human eye can receive [1].

Nevertheless, there are other compromises - for example, the time taken to integrate incoming light as the aircraft carrying the sensors moves. This means the raw airborne images appear deformed because the pixel length varies across the flightline. NERC-ARF geo-corrects the data using the Airborne Processing Library (APL) [13]. The processing levels are numbered. At ‘level 3’ (world coordinate system) the pixels are equally spaced and sized, which requires resampling and thus may look slightly blurred. The ‘level 1’ data (what the sensor saw) are non geo-corrected but they are associated with a file that defines the spatial location of each pixel. In this thesis, the ‘level 1’ data are used to preserve the highest possible quality.

In practise, the level 1 data are held in two files, the ‘.bil’ and the ‘.igm’. The ‘.bil’ file contains the hyperspectral cube (Figure 2-4), all the pixel values at different wavelengths, and the .igm file gives the x, y, z coordinates of each pixel.

The number of bands and the spectrum range captured depends on the hyperspectral sensor. The data from New Forest were collected using the following instruments:

- the Eagle, which captures the visible and near infra-red spectrum (400-970nm)
- the Hawk, which covers short wave infra-red wavelengths (970-2450nm)

Both sensors divide their spectral range into 252 bands (programmable) and each band is a 2D vector as shown in Figure 2-4).

The hyperspectral images also come with a number of drawbacks. A few are mentioned here but since hyperspectral imagery is not the main focus of the thesis there are not addressed:

- System faults sometimes occurs and the affected areas are masked out. This results in blank areas.

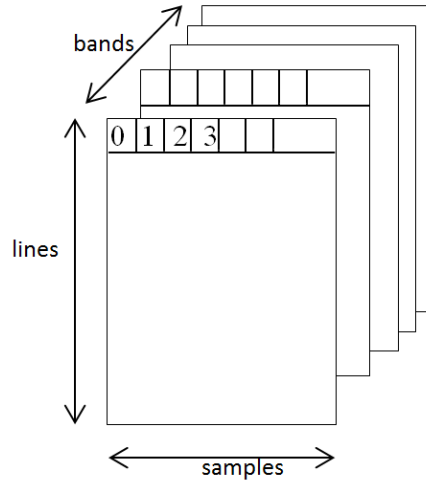


Figure 2-4: This figure shows the order of the hyperspectral pixels saved into the the binary .bil file.

- As a passive sensor, it is dependent on the sun for illumination and thus vulnerable to poor weather conditions
- Due to the high refraction of light at some wavelengths, some bands are highly influenced by humidity (i.e. wavelength 1898.33nm).

To sum up, hyperpsectral images contain information beyond the visible and they are delivered in two files, one contains the hyperspectral cube and the other one the geo-locations of each pixel. In this project, they are used in chapter (Chapter 7), where it is shown that the combination of Remote Sensing data confers better results for generating tree coverage maps.

Chapter 3

Overview of Thesis

Chapter 4

The open source software DASOS and the Voxelisation Approach

As mentioned in Section ??, there are very few uses of FW LiDAR data because of the quantity of the recorded information. For that reason, DASOS was developed (Section 4.3) as an open source software, to help foresters without computer science background to use FW LiDAR data while simultaneously advancing the research goals of this thesis. In this section:

- An overview of related software packages is given and we explain how DASOS differs from those packages (Section 4.1).
- The main method of interpreting the data within DASOS (the voxelisation approach) is described (Subsection 4.2).
- All the functionalities of DASOS are listed (Section 4.3)
- and, finally, a summary is provided (Section 4.4).

4.1 State-of-Art FW LiDAR Software Packages

The most common approach for interpreting FW LiDAR is the Gaussian decomposition of the waveforms for peak-points extraction. Each waveform is modelled as a set of Gaussian pulses and for every Gaussian peak, a single return (equivalent to a discrete LiDAR point) is extracted [14]. Neunschwander et al used this approach for Landcover classification [15] while Reitberger et al applied it for distinguishing deciduous trees from coniferous trees [16]. Chauve et al further proposed an approach of improving the Gaussian model in order to increase the density of the points extracted from the

data and consequently improve point based classifications of FW LiDAR data [6]. The following tools are able to extract discrete points from the waveforms and visualise small areas of interest:

- **Pulsewaves**: visualises a small number of waveforms using different transparencies according to the intensities of the wave-samples and is able to generate discrete point clouds [17].

Link: <<https://rapidlasso.com/pulsewaves/>>

- **FullAnalyze**: supports echo decomposition. Regarding visualisations, the user can select single trees from the Graphical User Interface (GUI) and, for each wave-sample, a sphere with radius proportional to its amplitude is created and visualised [18].

Link: <<http://fullanalyze.sourceforge.net/>>

- **SPDlib**: exports discrete LiDAR and visualises either the samples that are above a threshold level as points or the extracted discrete point cloud. It also colours them according to their intensity value [19].

Link: <<http://www.spdlib.org/>>

Echo decomposition and extraction of peak points identifies significant features and further enables the interpretation of the data within existing workflows and software that support discrete LiDAR data. For example, the discrete LiDAR can be analysed using:

- **Lag**: a visualisation tool for analysing and inspecting discrete LiDAR point clouds.

Link: <<http://arsf.github.io/lag/>>

- **Quick Terrain Modeller** : a 3D discrete LiDAR points visualiser, that can generate Digital Elevation Models (DEM) and Digital Terrain Models (DTM).

Link: <<http://appliedimagergy.com/>>

- **LASTools** : a tool set that classifies noise, visualises point clouds, clips data.

Link <<https://rapidlasso.com/lastools/>>

The DASOS approach to interpreting FW LiDAR data is fundamentally different from the aforementioned software packages. On the one hand, converting FW LiDAR into discrete peaks eases their usage, since existing workflows support discrete LiDAR. On the other hand, FW LiDAR contains information about pulse width that is not

preserved after peak point extraction. Also the comparison of point clouds depends on the density of the emitted pulses; problems arise with the sinusoidal scanning pattern of, for example, the Leica system, resulting in higher numbers of samples at the edges of the swath and lower in the middle. For these reasons, in DASOS, this information is accumulated from multiple shots into a voxel array, building up a 3D density volume. The correlation between multiple pulses in a voxel representation produces a more accurate and complete representation, which confers greater noise resistance and it further opens up possibilities of vertical interpretation of the data. The idea of voxelising FW LiDAR data is explained in the following section 4.2.

4.2 Voxelisation for Interpreting FW LiDAR data

The FW LiDAR data are voxelised by inserting the wave samples into a 3D regular grid and constructing a 3D discrete density volume. According to Persson et al, each wave sample is associated with the 3D cell, named voxel, that it lies inside. If multiple samples lie inside a voxel then the sample with the highest intensity is chosen [20]. In order to reduce noise, there are two differences between this approach and the way FW LiDAR data are voxelised in DASOS.

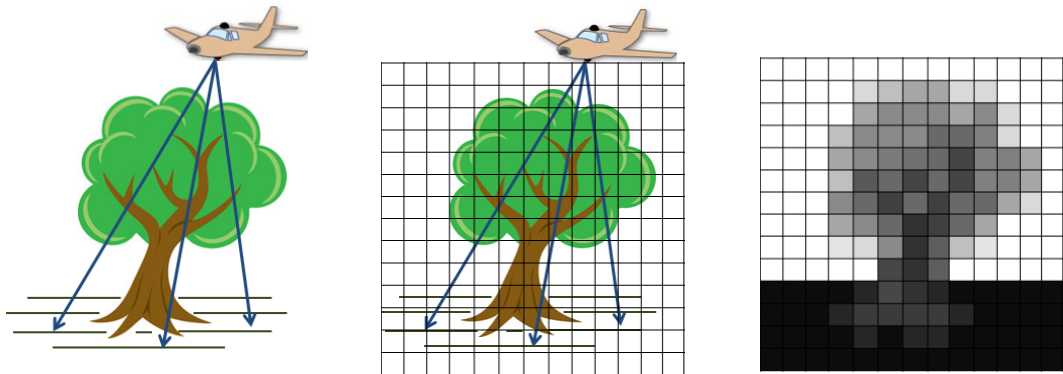
At first a threshold is used to remove low level noise, because when the length of a recorded waveform is longer than the distance between the first hit point and the ground, the system captures low signals for the remaining sampling time period after the pulse has been absorbed by the ground, which results pure noise. For that reason, the samples whose intensity is lower than a user-defined noise level/threshold are discarded.

As before, each wave sample is associated with the voxel that it lies inside. The second difference is how DASOS overcomes the uneven number of samples per voxels, which is primarily caused by the differing angle at which the LiDAR shot passes through voxels directly below the sensor and those off to the sides. The intensity of each sample is the laser intensity returned during the corresponding time interval. For example, if 5 samples are inside a voxel and the waveform is digitised at 2ns, then the laser intensity associated with that voxel corresponds to a 10ns waveform sampling length. For comparison purposes, it's essential to keep the waveform length consistent across the voxels. To overcome this issue in DASOS, the average intensity of the samples that lie inside each voxel is taken, instead of choosing the one with the highest intensity [20]. This way, the likelihood that the 3D volume will be affected by outliers and high noise is reduced. The following equation shows how the intensity value of a voxel is calculated:

$$I_v = \frac{\sum_{i=1}^n I_i}{n} \quad (4.1)$$

where I_v is the accumulated intensity of voxel v , n is number of samples associated with that voxel and I_i is the intensity of the sample i .

To sum up, during voxelisation, the area of interest is divided into voxels. The samples of the FW LiDAR data are inserted inside this 3D discrete density volume and normalised such that equally sized waveform length is saved inside each voxel. The result is a 3D discrete density volume of the scanned area. Figure 4-1 depicts this process in 2D.



(a) The sensor from the plane emits multiple pulses and collects information from the returned laser intensity.

(b) The area of interest is divided into equally sized cubes, named voxels, generating this way a discrete volume.

(c) The accumulated intensities of wave samples into the volume build up the voxelised representation of the scanned area.

Figure 4-1: The above images depict the voxelisation process of the FW LiDAR data in 2D. Please note that the voxelisation output in Figure 4-1c shows how ideally the result would look. But in reality, a number of trees may be disconnected from the ground due to missing information about their trunk.¹

¹The tree and plane images are taken from: <http://images.clipartpanda.com/tree-clip-artKij4jKriq.jpeg> & http://gmv.cast.uark.edu/wpcontent/uploads/2013/01/ALS_scematic.jpg

4.3 The functionalities of DASOS

So far, an overview of existing software packages supporting FW LiDAR was given (Section 4.1) and it was explained how DASOS differs from them by voxelising the waveforms (Section 4.2). In this section, the three main functionalities of DASOS are described in Tables 4.1, 4.2 and 4.3.

Each functionality is linked to a number of thesis sections, which describe the algorithms implemented and related applications. In a few words, the 3D visualisations are useful in forestry for reducing fieldwork and improving planning of field trips (e.g. checking whether a road passes through a fieldplot area). The 2D metrics allow simultaneous interpretation of FW LiDAR data and hyperspectral imagery. They could also be used in GIS software. In this thesis, they are used for generating tree coverage maps. Last but not least the priors enable 3D feature detection and they are used for detecting dead standing trees.

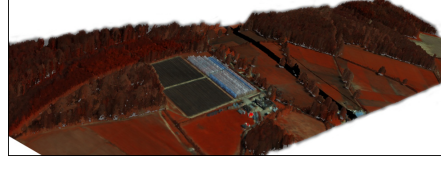
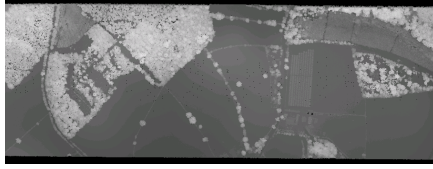
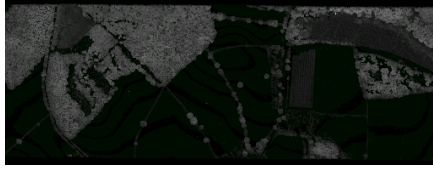
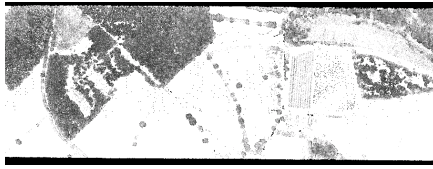
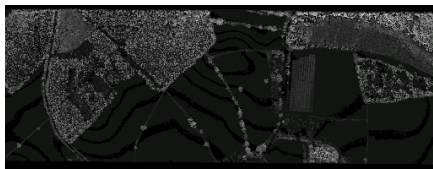
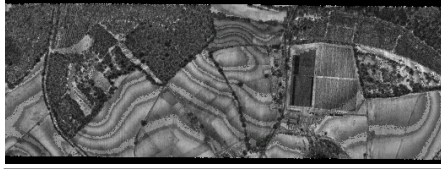
First Functionality: 3D Polygon Mesh Generation			
Input	Description	Output Example	Output Format
LAS1.3	3D Polygon Mesh Constructed from the volumetric representation (algorithms and user-defined parameters are explained in Section 5 while optimisation approaches are discussed in Section 6)		.obj
LAS1.3 and level 1 (.bil & .igm)	3D Coloured Polygon Mesh Projecting 3 user-defined hyperspectral bands on the mesh (Section 7)		.obj & .png

Table 4.1: The 1st functionality of DASOS that generates 3D polygonal meshes.

**Second Functionality: Generation of 2D metrics
aligned with hyperspectral imagery**

In Section 7 a selection of the following metrics are used
for generating tree coverage maps

Input	Metric Description (L for LiDAR metrics & H for hyperspectral metrics)	Output Example	Output Format
LAS1.3	L0 - Height: The distance between the top non-empty voxel and the lower boundaries of the volume.		.asc
LAS1.3	L1 - Thickness: The distance between the first and last non empty voxels in every column of the 3D volume.		.asc
LAS1.3	L2 - Density: Number of non-empty voxel over all voxels within the range from the first to last non-empty voxels.		.asc
LAS1.3	L3 - First Patch: The number of non-empty adjacent voxels, starting from the top non-empty voxel in that column.		.asc
LAS1.3	L4: Last Patch: The number of non-empty adjacent voxels, starting from the lower non-empty voxel in that column.		.asc

LAS1.3	L5 - Edge detection: The average height difference of neighbouring pixels.		.asc
LAS1.3	L6: Lowest Return The height of the lowest non empty voxel (the actual heights are very low and close to each but the example image has been scaled and the difference seems bigger)		.asc
LAS1.3	L7: Maximum Intensity The maximum intensity of each column		.asc
LAS1.3	L8: Average Intensity The average intensity per column		.asc
LAS1.3 and level 1 (.bil & .igm)	H0 : Mean The mean of the hyperspectral spectrum.		.asc
LAS1.3 and level 1 (.bil & .igm)	H1: Standard Deviation ¹ The standard deviation of the hyperspectral spectrum at each pixel.		.asc

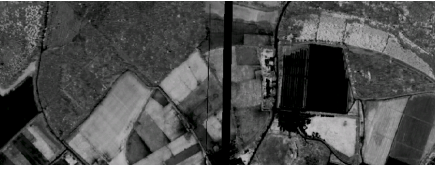
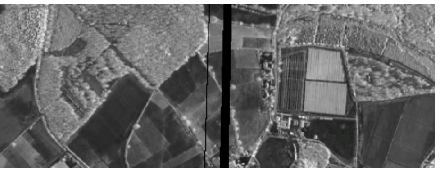
LAS1.3 and level 1 (.bil & .igm)	H2: NDVI The Normalised Difference Vegetation Index indicates whether green vegetation exists or not and it is derived from the electromagnetic spectrum as follow: $NDVI = \frac{NIR - VIS}{NIR + VIS} \quad (4.2)$ <p>where the NIR is the near-infrared region of the spectrum (700-2500nm) and VIS is the Visible/Visual spectrum (430-770) [25].</p>		.asc
LAS1.3 and level 1 (.bil & .igm)	H3: Spectral Signature ¹ The squared spectral difference between each pixels' spectrum and the generalised vegetation signature retrieved from USGS Digital Spectral Library [26].		.asc
LAS1.3 and level 1 (.bil & .igm)	H4: Band A single user defined hyperspectral band.	 	.asc .asc

Table 4.2: The 2nd functionality of DASOS that generates 2D metrics in ASCII format.

Third Functionality: 3D Priors / Signatures

The 3D priors/signatures characterise objects or local areas in 3D.
 In Section 8, the 3D priors are run over the volume
 for detecting dead standing trees

Input	Description	Output Example	Output Format
LAS1.3	3D Priors with raw intensities	Please Look at Figure 4-2	.csv
LAS1.3	3D Priors with processed intensities	Please Look at Figure 4-3	.csv

Table 4.3: The three functionalities of DASOS

Index	centroid_x	centroid_y	V0_0_0	V0_0_1	V0_0_2	V0_0_3	V0_0_4	V0_1_0	V0_1_1	V0_1_2	V0_1_3	...
0	251836.109	6048994.5	7	14	10	26	0	0	9	10.25	11.875	...
1	251843.906	6048980.5	0	0	0	0	0	0	0	0	0	...
2	251846.312	6048979	9	60.75	70.75	13	8	0	0	0	7.667	...
3	251849.312	6049022.5	48.556	93.222	20.5	0	7	0	0	0	0	...
4	251851.703	6048988	100.2	53.222	10.5	7.143	0	0	0	0	47.25	...
5	251852.906	6048975	0	0	0	0	0	26.875	0	10.444	13.182	...
6	251857.109	6048974	0	0	0	0	0	45.667	93	16.333	7.25	...
7	251858.312	6049010.5	0	0	0	0	0	0	0	8	6	...
8	251860.703	6048984	0	45.75	8	7.333	0	0	0	0	6.8	...
9	251861.312	6049000	0	0	0	0	0	0	0	0	0	...

Figure 4-2: Example of .csv files with priors exported. These priors contain the raw intensities of the voxels.

Index	centroid_x	centroid_y	Height_Middle_Column	Height_Mean	Height_Median	Height_Std	Sum_Int	Diff_X	...
0	251836.109	6048994.5	36	35.5	36	0.943	95.125	...	
1	251843.906	6048980.5	19.8	20.1	20.4	0.671	0	...	
2	251846.312	6048979	16.8	16	15.6	1.02	169.167	...	
3	251849.312	6049022.5	36	35.7	36.6	0.964	169.278	...	
4	251851.703	6048988	17.4	16.2	16.2	0.346	408.065	...	
5	251852.906	6048975	27	26.4	26.4	0.917	68.537	...	
6	251857.109	6048974	17.4	17.4	18	0.849	162.25	...	
7	251858.312	6049010.5	40.8	40	39.6	1.02	251.36	...	
8	251860.703	6048984	17.4	16.6	16.2	0.663	67.883	...	
9	251861.312	6049000	19.8	20.1	20.4	0.671	0	...	

Figure 4-3: Example of .csv files with priors exported. These priors contains proccesed information about the the local area of interest (i.e. spread of non empty voxels).

¹The marked metrics of Table 4.2 were implemented specifically for the tree coverage maps [24] and they are not available on the released version of DASOS.

It is further worth stating that detailed information about DASOS is provided at: <<http://miltomiltiadou.blogspot.co.uk/2015/03/las13vis.html>>. This link also indicates how to download DASOS, the complete user-guide and the source code, as well as where to seek support while using it.

4.4 Summary and Discussion

Along with supporting the research in this thesis, the open source software DASOS was developed to encourage foresters to use FW LiDAR data. The main way of interpreting FW LiDAR data in DASOS is fundamentally different from the state-of-art available software packages. In a few words, the FW LiDAR data are voxelised by inserting the wave samples into a 3D discrete density volume, which preserves an extra parameter (the echo width) in comparison to point extraction algorithms. It also accumulates intensity values from multiple shots and stores them into a 3D regular grid, resolving this way the problem with the sinusoidal footprint / uneven scanning pattern of the Leica system.

There are three main functionalities of DASOS: the construction of 3D polygon meshes, the generation of 2D metrics aligned with hyperspectral images and characterisation of objects using 3D priors/signatures. The visualisation outputs are also state-of-art since previous visualisations talk about points [19] or spheres [18], while DASOS is able to create closed polygon representation. In addition, the integration of various sensors allows simultaneous interpretation of their data and, in section 7, it is shown that this confers better results for generating tree coverage maps. The 3D priors allow local inspection of data and they are used in section 8 for dead standing tree detection in native Australian forests.

Finally, it worth mentioning that there a few individuals/organisation that showed interest in using DASOS and, in the future, usage of it, its derivatives or the concepts employed in it are expected to increase in remote forest surveys (i.e. for commercial forest stocking estimation or for infected trees detection and treatment).

Chapter 5

Surface Reconstruction from Voxelised FW LiDAR Data

Chapter 6

Optimisation Attempts for the Surface Reconstruction

Chapter 7

Alignment with Hyperspectral Imagery

Chapter 8

Detection of Dead Standing Eucalyptus For Managing Biodiversity in Native Australian Forest

Chapter 9

Overall Results

Chapter 10

Conclusions

10.1 Contributions

Bibliography

- [1] R. B. Smith, *Introduction to Hyperspectral Imaging*. MicroImages, 2014.
- [2] W. Wanger, A. Ullrich, T. Melzer, C. Briese, and K. Kraus, “From single-pulse to full-waveform airborne laser scanners,” *ISPRS Journal of Photogrammetry and Remote Sensing*, vol. 60, pp. 100–112, 2004.
- [3] A. Wehr and U. Lohr, “Airborne laser scanning - an introduction and overview,” *ISPRS Journal of Photogrammetry and Remote Sensing*, vol. 54, pp. 68–82, 1999.
- [4] C. Mallet and F. Bretar, “Full-waveform topographic lidar: State-of-the-art,” *ISPRS Journal of Photogrammetry and Remote Sensing*, vol. 64, pp. 1–16, 2009.
- [5] K. Anderson, S. Hancock, M. Disney, and K. Gaston, “Is waveform worth it? a comparison of lidar approaches for vegetation and landscape characterization,” *Remote Sensing in Ecology and Conservation*, 2015.
- [6] A. Chauve, C. Mallet, F. Bretar, S. Durrieu, M. Deseilligny, and W. Puech, “Processing full-waveform lidar data: Modelling raw signals,” *International Archives of Photogrammetry, Remote Sensing and Spatial Information Sciences*, 2007.
- [7] *LAS Specification version 1.3-R1*. Bethesda, Maryland: American Society for Photogrammetry and Remote Sensing, 2010.
- [8] M. Warren, *Full Waveform Upgrade*. NERC ARSF wiki, 2012.
- [9] M. J. Sumnall, R. A. Hill, and S. A. Hinsley, “Comparison of small-footprint discrete return and full waveform airborne lidar data for estimating multiple forest variables,” *Remote Sensing of Environment*, vol. 173, pp. 214–223, 2016.
- [10] K. H. R. A. Z. A. Lehner, H., “Consideration of laser pulse fluctuations and automatic gain control in radiometric calibration of airborne laser scanning data.,” *Proceedings of 6th ISPRS Student Consortium and WG VI/5 Summer School*, 2011.

- [11] I. Korpela, H. O. Ørka, H. V. Hyppä, J., and T. Tokola, “Range and agc normalization in airborne discrete-return lidar intensity data for forest canopies,” vol. 65, no. 4, pp. 369–379, 2010.
- [12] M. Isenburg, *LAStools - efficient tools for LiDAR processing*. rapidlasso.
- [13] M. Warren, B. Taylor, M. Grant, and J. D. Shutler, “Data processing of remorely sensed airborne hyperspectral data using the airborne processing library (apl),” *ScienceDirect, Computers and Geosciences*, vol. 64, 2014.
- [14] W. Wanger, A. Ullrich, V. Ducic, T. Maizer, and N. Studnicka, “Gaussian decompositions and calibration of a novel small-footprint full-waveform digitising airborne laser scanner,” *ISPRS Journal of Photogrammetry and Remote Sensing*, vol. 60, pp. 100–112, 2006.
- [15] A. Neuenschwander, L. Magruder, and M. Tyler, “Landcover classification of small-footprint full-waveform lidar data,” *Jounal of Applied Remote Sensing*, vol. 3, no. 1, pp. 033544–033544.
- [16] J. Reitberger, P. Krzystek, and U. Stilla, “Analysis of full waveform LiDAR data for tree species classification,” *International Journal of Remote Sensing*, vol. 29, no. 5, pp. 1407–1431, 2008.
- [17] M. Isenburg, “Pulsewaves: An open, vendor-neutral, stand-alone, las-compatible full waveform lidar standard.,” 2012.
- [18] A. Chauve, F. Bretar, S. Durrieu, M. Pierrot-Deseilligny, and W. Puech, “Fullanalyse: A research tool for handling, processing and analysing full-waveform lidar data,” *IEEE International Geoscience and Remote Sensing Symposium*, 2009.
- [19] P. Bunting, J. Armston, D. Clewley, and R. M. Lucas, “Sorted pulse data (spd) library—part ii: A processing framework for lidar data from pulsed laser systems in terrestrial environments,” *Computers & Geosciences*, vol. 56, pp. 207–215, 2013.
- [20] A. Persson, U. Soderman, J. Topel, and S. Ahlberg, *Visualisation and Analysis of full-waveform airborne laser scanner data*. V/3 Workshop, Laser scanning 2005, 2005.
- [21] L. Cao, N. Coops, L. Innes, J. Dai, and H. Ruan, “Tree species classification in subtropical forests using small-footprint full-waveform lidar data,” *International Journal of Applied Earth Observation and Geoinformation*, vol. 49, pp. 39–51, 2016.

- [22] S. Hancock, K. Anderson, M. Disney, and K. J. Gaston, “Measurement of fine-spatial-resolution 3d vegetation structure with airborne waveform lidar: Calibration and validation with voxelised terrestrial lidar,” *Remote Sensing of Environment*, vol. 188, pp. 37–50, 2017.
- [23] M. Miltiadou, M. Grant, M. Brown, M. Warren, and E. Carolan, “Reconstruction of a 3d polygon representation from full-waveform lidar data,” *RSPSoc Annual Conference 2014, New Sensors for a Changing World*, 2014.
- [24] M. Miltiadou, M. A. Warren, M. Grant, and M. Brown, “Alignment of hyperspectral imagery and full-waveform lidar data for visualisation and classification purposes,” *The International Archives of Photogrammetry, Remote Sensing and Spatial Information Sciences*, vol. 40, no. 7, p. 1257, 2015.
- [25] R. Crippen, “Calculating the vegetation index faster,” *Remote Sensing of Environment*, vol. 34, no. 1, pp. 71–73, 1990.
- [26] R. N. Clark, G. A. Swayze, R. Wise, K. E. Livo, T. Hoefen, R. F. Kokaly, and S. J. Sutley, “Usgs digital spectral library splib06a,” *US Geological Survey, Digital Data Series*, vol. 231, 2007.

Appendix A

DASOS user guide

Appendix B

Case Study: Field Work in New Forest